Impact of Phase-Noise and Spatial Correlation on Double-RIS-Assisted Multiuser MISO Networks

Zaid Abdullah, *Member, IEEE*, Anastasios Papazafeiropoulos, *Senior Member, IEEE*, Steven Kisseleff, *Member, IEEE*, Symeon Chatzinotas, *Senior Member, IEEE*, and Björn Ottersten, *Fellow, IEEE*

***Abstract*—We study the performance of a phase-noise impaired double reconfigurable intelligent surface (RIS)-aided multiuser (MU) multiple-input single-output (MISO) system under spatial correlation at both RISs and base-station (BS). The downlink achievable rate is derived in closed-form under maximum ratio transmission (MRT) precoding. In addition, we obtain the optimal phase-shift design at both RISs in closed-form for the considered channel and phase-noise models. Numerical results validate the analytical expressions, and highlight the effects of different system parameters on the achievable rate. Our analysis shows that phase-noise can severely degrade the performance when users do not have direct links to both RISs, and can only be served via the double-reflection link. Also, we show that high spatial correlation at RISs is essential for high achievable rates.**

***Index Terms*—Reconfigurable intelligent surface (RIS), phase-noise, channel correlation, multiuser communication.**

I. Introduction

TODAY, there is no lack of interest among researchers around the globe when it comes to the potential of reconfigurable intelligent surfaces (RISs) [1]. This does not come as a surprise since the concept of RIS shattered the old belief that the response of a wireless channel cannot be altered. Also, a great benefit of this technology lies in the fact that RISs are considered as energy green nodes since no (or limited number of) radio-frequency chains are required for their operations, and no power amplification is involved [2].

Despite the large volume of existing research on RISs, most of the works considered a single RIS-assisted network. However, in practical scenarios, signals can be subject to reflections from multiple spatially-separated RISs [3]. To that end, the authors in [4] studied a cooperative beamforming design of a multiuser (MU) system based on instantaneous channel state information (iCSI), and the estimation process of such iCSI for different communication links in the double-RIS networks was demonstrated in [5]. The authors in [6] derived the coverage probability of a single-input single-output (SISO) double-RIS network with statistical CSI (sCSI)-based reflect beamforming design (RBD), where the optimization of phase-shifts at RISs is performed without requiring any knowledge of iCSI. Note that such approach is very useful in practice as the amount of training required to estimate all different channels in multiple RISs networks can become very large with respect to the coherence interval of a wireless channel.

Another practical aspect is the hardware impairments (HWIs), which cannot be avoided in realizing any communication system. Specifically, two main types of HWIs have been highlighted in the literature regarding the implementation of RISs. The first one is the discrete phase-shifts [2], where only few quantization levels of reflecting coefficients can be obtained; while the second type of HWIs is the phase-noise, which reflects imperfections in phase-estimation and/or phase-quantization [7]. The latter will be the focus of this letter. Few works have investigated the phase-noise in RIS-assisted networks so far. For example, the authors in [7] and [8] thoroughly analyzed the performance of a point-to-point SISO system assisted by a RIS impaired with phase-noise under fading and non-fading (i.e., line-of-sight) channels, respectively. In addition, the works in [9] and [10] studied the performance of an MU multiple-input single-output (MISO) system assisted by a single RIS under HWIs, where the gradient ascent method was adopted for the RIS RBD. In [11] the authors investigated the achievable rate of a RIS assisted SISO network with HWIs, where the RBD problem was tackled via the semidefinite relaxation approach. Finally, the work in [12] investigated the spectral and energy efficiencies of a single-user MISO network aided by an imperfect RIS, and their results showed that HWIs limit the spectral efficiency even when the number of reflecting elements grows to infinity.

All previous works considered the impact of HWIs on a single-RIS network. In contrast, here we analyze the achievable rate of a double-RIS assisted MU-MISO network under phase-noise impacting both RISs. In addition, we obtain a closed-form solution for the optimal RBD and shed light into the role of spatial correlation at both the base-station (BS) and RISs, and their effect on the achievable rate. Our contributions are summarized as follows:

- We derive a closed-form expression for the achievable rate of correlated and phase-noise impaired double-RIS MU-MISO network under maximum ratio transmission (MRT) precoding at BS and optimized RBD at both RISs.
- We demonstrate that the spatial correlation at RISs leads to higher channels gain, thereby resulting in an improved rate performance, while the transmit correlation at BS has a negative impact on the achievable rates.
- In addition, we prove that based on sCSI, the phase-shift matrices at both RISs that lead to a maximum achievable rate can be obtained in closed-form without the need for any sophisticated optimization tools.

Manuscript received April 17, 2022; accepted May 12, 2022. Date of publication May 17, 2022; date of current version July 11, 2022. This work was supported by the Luxembourg National Research Fund through the CORE Project under Grant RISOTTI C20/IS/14773976. The associate editor coordinating the review of this article and approving it for publication was Y. Fu. *(Corresponding author: Zaid Abdullah.)*

Zaid Abdullah, Steven Kisseleff, Symeon Chatzinotas, and Björn Ottersten are with the Interdisciplinary Center for Security, Reliability and Trust (SnT), University of Luxembourg, 1855 Luxembourg City, Luxembourg (e-mail: zaid.abdullah@uni.lu; steven.kisseleff@uni.lu; symeon.chatzinotas@uni.lu; bjorn.ottersten@uni.lu).

Anastasios Papazafeiropoulos is with the Communications and Intelligent Systems Research Group, University of Hertfordshire, Hatfield AL10 9AB, U.K., and also with Interdisciplinary Center for Security, Reliability and Trust, University of Luxembourg, 1855 Luxembourg City, Luxembourg (e-mail: tapapazaf@gmail.com).

Digital Object Identifier 10.1109/LWC.2022.3175539

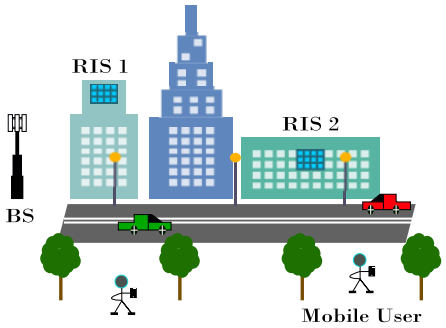

Fig. 1. The considered double RIS communication system in a scattering environment.

To the best of our knowledge, these aspects have not been investigated so far in the literature.

The rest of this letter is organized as follows: Section II presents the system model. Section III analyzes the achievable rate and RBD. Section IV presents the numerical results and their discussion. Conclusions are drawn in Section V.

Notations: Matrices and vectors are denoted by boldface uppercase and lowercase letters, respectively. $\boldsymbol{a}^T$, $\boldsymbol{a}^H$, $\boldsymbol{a}^*$, and $\|\boldsymbol{a}\|$ are the transpose, Hermitian transpose, conjugate, and Euclidean norm of a vector $\boldsymbol{a}$, respectively. $\boldsymbol{I}_N$ is the $N \times N$ identity matrix, while $[\boldsymbol{A}]_{i,j}$ is the (i, j)th entry of $\boldsymbol{A}$, and $[\boldsymbol{a}]_i$ is the ith element of $\boldsymbol{a}$. The absolute, expected, and trace operators are denoted by $|\cdot|$, $\mathbb{E}\{\cdot\}$, and $\text{tr}(\cdot)$, respectively. Furthermore, $\text{diag}\{\boldsymbol{a}\}$ is a diagonal matrix whose diagonal contains the elements of $\boldsymbol{a}$, while $\text{diag}\{\boldsymbol{A}\}$ is a vector whose elements are the diagonal of $\boldsymbol{A}$. Finally, $\Re\{x\}$ denotes the real part of a complex number x.

II. System Model

A. Signal, Channel, and Phase-Noise Models

We consider a time-division-duplex MU downlink scenario where there is one BS consisting of a uniform linear array (ULA) with M active radiating elements, communicating with K single-antenna users $\{U_1, \ldots, U_K\}$. We focus on a challenging, but meaningful scenario that justifies the presence of RISs where the direct path between the BS and all K users is assumed to be blocked, and communication is facilitated via two RISs (I_1 and I_2) equipped with N_1 and N_2 reflecting elements, respectively, as shown in Fig. 1. A rectangular geometry is adopted for each RIS with N_{V_i} vertical and N_{H_i} horizontal elements, such that $N_i = N_{V_i} N_{H_i}$, $i \in \{1, 2\}$. Assuming that all communication links experience flat fading, the received signal at kth user is

$$y_k = \boldsymbol{h}_k^T \boldsymbol{w}_k x_k + \sum_{l \in \mathcal{U} \setminus k} \boldsymbol{h}_k^T \boldsymbol{w}_l x_l + z_k, \tag{1}$$

where $\mathcal{U} = \{1, \ldots, K\}$, x_k is the information symbol intended for kth user satisfying $\mathbb{E}\{|x_k|^2\} = p_k$ with p_k being the power allocated for kth user, such that $\sum_{k \in \mathcal{U}} p_k \leq P_t$, where P_t is the total power available at BS. Also, $z_k \sim \mathcal{CN}(0, \sigma^2)$ is the additive white Gaussian noise (AWGN) at U_k, $\boldsymbol{w}_k = \frac{\boldsymbol{h}_k^*}{\sqrt{\mathbb{E}\{\|\boldsymbol{h}_k\|^2\}}} \in \mathbb{C}^{M \times 1}$ is the MRT beamforming vector at BS for U_k, and $\boldsymbol{h}_k \in \mathbb{C}^{M \times 1}$ is the effective channel vector for the same user given as[1]

$$\boldsymbol{h}_k = \boldsymbol{H}_{B1} \tilde{\boldsymbol{\Theta}}_1 \boldsymbol{G} \tilde{\boldsymbol{\Theta}}_2 \boldsymbol{q}_{2k} + \boldsymbol{H}_{B1} \tilde{\boldsymbol{\Theta}}_1 \boldsymbol{q}_{1k} + \boldsymbol{H}_{B2} \tilde{\boldsymbol{\Theta}}_2 \boldsymbol{q}_{2k}, \tag{2}$$

where the first term in (2) accounts for double reflection link,[2] while the second and third terms account for single reflection links through the first and second RISs, respectively. In particular, $\boldsymbol{q}_{ik}$ is the vector of channel coefficients between $I_i \to U_k$, such that $\boldsymbol{q}_{ik} = \sqrt{\beta_{ik}} \boldsymbol{R}_i^{\frac{1}{2}} \tilde{\boldsymbol{q}}_{ik} \in \mathbb{C}^{N_i \times 1}$, with $\tilde{\boldsymbol{q}}_{ik} \sim \mathcal{CN}(\boldsymbol{0}, \boldsymbol{I}_{N_i}) \in \mathbb{C}^{N_i \times 1}$ being a vector containing independent and identically distributed (i.i.d.) Rayleigh fading components, while $\boldsymbol{R}_i \in \mathbb{C}^{N_i \times N_i}$ is the Hermitian positive semidefinite correlation matrix for the ith RIS with $\text{tr}(\boldsymbol{R}_i) = N_i$, and β_{ik} is the channel gain between each reflecting element at I_i and U_k given as $\beta_{ik} = d_{ik}^{-\alpha} A$ [14], where $A = d_V d_H$ is the area of each reflecting element with d_V and d_H being the vertical height and horizontal width, d_{ik} is the distance between I_i and U_k, and α is the path-loss exponent. On the other hand, $\boldsymbol{H}_{Bi} \in \mathbb{C}^{M \times N_i}$ is a matrix containing channel coefficients between BS and I_i. Specifically, we have $\boldsymbol{H}_{Bi} = \sqrt{\beta_{Bi}} \boldsymbol{R}_B^{\frac{1}{2}} \tilde{\boldsymbol{H}}_{Bi} \boldsymbol{R}_i^{\frac{1}{2}}$, where $\beta_{Bi} = d_{Bi}^{-\alpha} A$ is the channel gain between BS and each reflecting element at I_i, $\boldsymbol{R}_B \in \mathbb{C}^{M \times M}$ is a Hermitian positive semidefinite matrix that accounts for the antenna correlation at the BS with $\text{tr}(\boldsymbol{R}_B) = M$, and $\text{vec}(\tilde{\boldsymbol{H}}_{Bi}) \sim \mathcal{CN}(\boldsymbol{0}, \boldsymbol{I}_{MN_i})$ is the i.i.d Rayleigh fading components. Similarly, we have $\boldsymbol{G} = \sqrt{\beta_G} \boldsymbol{R}_1^{\frac{1}{2}} \tilde{\boldsymbol{G}} \boldsymbol{R}_2^{\frac{1}{2}} \in \mathbb{C}^{N_1 \times N_2}$ contains the correlated Rayleigh fading channel coefficients between the two RISs with $\text{vec}(\tilde{\boldsymbol{G}}) \sim \mathcal{CN}(\boldsymbol{0}, \boldsymbol{I}_{N_1 N_2})$, and $\beta_G = d_{1,2}^{-\alpha} A^2$ is the corresponding channel gain with $d_{1,2}$ being the distance between the two RISs.

Moreover, for the phase-shift matrix of ith RIS ($i \in \{1, 2\}$), we have $\tilde{\boldsymbol{\Theta}}_i = \bar{\boldsymbol{\Theta}}_i \boldsymbol{\Theta}_i \in \mathbb{C}^{N_i \times N_i}$, whereas $\boldsymbol{\Theta}_i = \text{diag}\{[e^{\jmath[\boldsymbol{\theta}_i]_1}, e^{\jmath[\boldsymbol{\theta}_i]_2}, \ldots, e^{\jmath[\boldsymbol{\theta}_i]_{N_i}}]\}$ is the diagonal phase-shift matrix, while $\bar{\boldsymbol{\Theta}}_i = \text{diag}\{[e^{\jmath[\bar{\boldsymbol{\theta}}_i]_1}, e^{\jmath[\bar{\boldsymbol{\theta}}_i]_2}, \ldots, e^{\jmath[\bar{\boldsymbol{\theta}}_i]_{N_i}}]\}$ accounts for the phase-noise errors at the ith RIS. Similar to [7]–[9], the phase-noise, captured by $\bar{\boldsymbol{\Theta}}_1$ and $\bar{\boldsymbol{\Theta}}_2$, can be modeled according to the Von Mises (VM) distribution with zero-mean and a characteristic function (CF) $\mathbb{E}\{e^{\jmath[\bar{\boldsymbol{\theta}}_i]_n}\} = \frac{I_1(\kappa)}{I_0(\kappa)} = \varphi$, where $I_p(\kappa)$ is the modified Bessel function of first kind and order p, and κ is the concentration parameter accounting for the estimation accuracy.

B. Spatial Correlation Models

Here, we introduce the adopted spatial correlation models for BS and both RISs.

1) Spatial Correlation at BS: We apply the Kronecker correlation model [15] at the BS, which is suitable for uniform linear arrays, such that the (i, j)th entry of $\boldsymbol{R}_B$ is given as

$$[\boldsymbol{R}_B]_{i,j} = \begin{cases} \rho^{(j-i)}, & \text{if } i \leq j \\ (\rho^{|j-i|})^*, & \text{otherwise,} \end{cases} \qquad \forall \{i, j\} \in \mathcal{M}, \tag{3}$$

where $\rho \in \mathbb{C}$ is the correlation coefficient satisfying $|\rho| \leq 1$, and $\mathcal{M} = \{1, 2, \ldots, M\}$.

2) Spatial Correlation at RISs: For each RIS, we utilize the spatial correlation proposed by [14] for rectangular surfaces. In particular, the (l, m)th entry of $\boldsymbol{R}_i$ is given as

$$[\boldsymbol{R}_i]_{l,m} = \text{sinc}\left(\frac{2\|\boldsymbol{u}_{i_l} - \boldsymbol{u}_{i_m}\|}{\lambda} \right), \qquad \forall \{l, m\} \in \mathcal{N}_i, \tag{4}$$

[1]To focus on the effects of phase-noise and spatial correlation, we assume perfect knowledge of CSI for the overall effective channel vector $\boldsymbol{h}_k$, while it can be obtained via traditional estimation techniques in practice [13]. Thus, our results represent an upper-bound for imperfect CSI scenarios.

[2]There exists a path from BS $\to I_2 \to I_1 \to U_k$. However, its gain is sufficiently weaker than that from BS $\to I_1 \to I_2 \to U_k$ shown in (2), since I_1 is closer to BS than I_2, and thus the former path can be neglected.

where $\|\boldsymbol{u}_{i_l} - \boldsymbol{u}_{i_m}\|$ is the distance between lth and mth reflecting elements at I_i,[3] λ is the wavelength, and $\mathcal{N}_i = \{1, 2, \ldots, N_i\}$.

III. Achievable Rate Analysis and Optimization

Here, we formulate the received signal-to-interference-plus noise ratios (SINRs) and provide closed-form expressions for the achievable rate and optimal RBD.

A. Received SINR and Achievable Rate

Given that the instantaneous received SINR for kth user is

$$\mathrm{SINR}_k = \frac{p_k \left| \boldsymbol{h}_k^T \boldsymbol{w}_k \right|^2}{\sum_{l \in \mathcal{U} \setminus k} p_l \left| \boldsymbol{h}_k^T \boldsymbol{w}_l \right|^2 + \sigma^2}, \tag{5}$$

the ergodic rate for the same user can be expressed as $\mathcal{R}_k = \mathbb{E}\{\log_2(1+\mathrm{SINR}_k)\}$. However, since obtaining a closed-form expression for $\mathcal{R}_k$ is mathematically challenging, we follow a similar approach to that in [13] which takes advantage of channel hardening, and derive the lower-bound achievable rate as demonstrated in the following Theorem.

Theorem 1: For a given $\boldsymbol{\Theta}_1$ and $\boldsymbol{\Theta}_2$, the downlink achievable rate for U_k with MRT precoding and phase-noise is

$$\underline{\mathcal{R}}_k = \log_2(1 + \underline{\mathrm{SINR}}_k) \tag{6}$$

with

$$\underline{\mathrm{SINR}}_k = \frac{p_k M^2}{\mathrm{tr}\big(\boldsymbol{R}_B^2\big)\big(\sum_{l \in \mathcal{U}} p_l\big) + \frac{M\sigma^2}{\eta_k}}, \tag{7}$$

where η_k is given in a closed-form as

$$\begin{aligned}\eta_k = \beta_{B1}\beta_{2k}\beta_G \Big[\mathrm{tr}\big(\boldsymbol{R}_2 \bar{\boldsymbol{R}}_2\big) \Big(\varphi^4 \mathrm{tr}\big(\boldsymbol{R}_1 \bar{\boldsymbol{R}}_1\big) + (\varphi^2 - \varphi^4) N_1 \Big) \\ + N_2 \Big((\varphi^2 - \varphi^4) \mathrm{tr}\big(\boldsymbol{R}_1 \bar{\boldsymbol{R}}_1\big) + (1-\varphi^2)^2 N_1 \Big) \Big] \\ + \sum_{i=1}^{2} \beta_{Bi}\beta_{ik} \Big(\varphi^2 \mathrm{tr}\big(\boldsymbol{R}_i \bar{\boldsymbol{R}}_i\big) + (1-\varphi^2) N_i \Big)\end{aligned} \tag{8}$$

with $\bar{\boldsymbol{R}}_i = \boldsymbol{\Theta}_i \boldsymbol{R}_i \boldsymbol{\Theta}_i^H$.

Proof: See the Appendix.

Remark 1: The expression of SINR in (7) demonstrates that while spatial correlation at the BS is harmful,[4] the correlation at both RISs can in fact be utilized to enhance the achievable SINR by maximizing η_k. In fact, we will prove in the following subsection that under optimal RBD the achievable rate increases with the correlation level at each RIS, as higher correlation can always lead to increased values of η_k.

Remark 2: When $\varphi = 0$ (which corresponds to a VM noise concentration parameter of $\kappa = 0$), the optimization of $\boldsymbol{\Theta}_1$ and $\boldsymbol{\Theta}_2$ would not lead to any performance enhancement, and both RISs can only reflect the impinging signal without any phase-adjustment capabilities. This can be further illustrated by the probability density function formula of the VM noise given as $f(r|\kappa) = \frac{e^{\kappa \cos(r)}}{2\pi I_0(\kappa)}$ with $r \in [-\pi, \pi]$ [8]. Clearly, when $\kappa = 0$, the VM phase-noise will be evenly distributed over the period $[-\pi, \pi]$, and hence, no useful information regarding the phase-estimation can be obtained to facilitate the RBD. This is in line with the findings of [8] and [9] for the single RIS case. However, for the double RIS, we can still benefit from the additional $\beta_{B1}\beta_{2k}\beta_G N_1 N_2 + \beta_{B2}\beta_{2k} N_2$ channel gain compared to the single RIS case where only I_1 exists (in such case the channel gain would be $\beta_{B1}\beta_{1k} N_1$), as demonstrated by (8).

Finally, it is also observed from (8) that the double reflection link is the most affected by the phase-noise in terms of φ^4, compared to φ^2 for single reflection links.[5] Thus, for scenarios where users can only be served by the double-reflection link, the performance of multi-RIS networks can be severely degraded by phase-noise errors.

We next shift our attention to the phase-shift design of both RISs.

B. Phase-Shift Design

Our aim is to optimize $\boldsymbol{\Theta}_1$ and $\boldsymbol{\Theta}_2$, based on only sCSI,[6] to maximize the achievable rate in (6) for all users. We start by formulating the problem as

$$\underset{\boldsymbol{\Theta}_1,\, \boldsymbol{\Theta}_2}{\text{maximize}} \ \sum_{k \in \mathcal{U}} \underline{\mathcal{R}}_k \tag{9}$$

$$\text{subject to } \big|[\boldsymbol{\Theta}_i]_{n,n}\big| = 1, \quad \forall n \in \mathcal{N}_i, \quad i \in \{1,2\}. \tag{9a}$$

Interestingly, from (7) we can observe that the only term related to the phase-shift matrices is η_k. Thus, in order to maximize the achievable rate, we only need to maximize η_k ($\forall k \in \mathcal{U}$). Now, we can further introduce the following Corollary.

Corollary 1: The maximization of the achievable rate is equivalent to the maximization of $\mathrm{tr}(\boldsymbol{R}_i \boldsymbol{\Theta}_i \boldsymbol{R}_i \boldsymbol{\Theta}_i^H)$ for both $i = \{1, 2\}$.

Proof: Given that the characteristic function of the VM noise satisfies $0 \leq \varphi \leq 1$, it holds that $\varphi^p \geq \varphi^n$ for all $p \leq n$, and $\{p, n\}$ are positive integers. Thus, maximizing η_k is equivalent to maximizing the term $u_k = c_{0k} v_2 v_1 + c_{1k} v_1 + c_{2k} v_2 + c_{3k}$, with the optimization variables v_1 and v_2 being $\mathrm{tr}(\boldsymbol{R}_1 \boldsymbol{\Theta}_1 \boldsymbol{R}_1 \boldsymbol{\Theta}_1^H)$ and $\mathrm{tr}(\boldsymbol{R}_2 \boldsymbol{\Theta}_2 \boldsymbol{R}_2 \boldsymbol{\Theta}_2^H)$, respectively, and $\{c_{0k}, \ldots, c_{3k}\}$ are constants belonging to the set of positive real numbers $\mathbb{R}_{++}$.

Clearly, u_k is maximum if and only if both v_1 and v_2 are maximum, which indicates that both variables should belong to $\mathbb{R}_{++}$. Moreover, since maximizing v_1 does not depend on v_2, and vice-versa, optimizing each of v_1 and v_2 separately would also result in both variables being jointly optimal in terms of their sum and product. Therefore, and given that v_1 and v_2 are independent of the user index, it holds that maximizing both variables separately, via phase-optimization, will result in the optimal achievable sum rate. This concludes our proof.

Interestingly, Corollary 1 shows that the phase optimization of different RISs in a multiple RIS-assisted scenario can be performed separately under sCSI, and without any loss of optimality. Next, for optimal RBD, we introduce the following Theorem.

Theorem 2: The optimal solution for $\boldsymbol{\Theta}_i$ ($i \in \{1,2\}$) that maximizes $\mathrm{tr}(\boldsymbol{R}_i \boldsymbol{\Theta}_i \boldsymbol{R}_i \boldsymbol{\Theta}_i^H)$, and hence the achievable sum rate, must satisfy $\boldsymbol{\Theta}_i^\star = \mathrm{diag}\{\exp(\jmath c \mathbf{1}_{N_i})\}$, where $c \in \mathbb{R}$ is

[3] We denote the distance between two adjacent elements at the RIS as ε.

[4] Here, we consider a transmit correlation model, which reflects the spatial correlation at the BS due to limited spacing among different antenna elements and/or insufficient scattering, and such correlation is independent of the user. However, local scattering-based channel correlation where each user experience different spatial correlation with BS can in fact lead to an enhanced rate performance [13].

[5] Note that $0 \leq \varphi \leq 1$ with $\varphi = 1$ corresponding to an ideal case without any phase-noise.

[6] Utilizing only sCSI to perform the RBD is highly efficient in terms of the amount of training required as only the overall cascaded channel needs to be estimated, while it leads to sub-optimal performance in terms of received SINRs compared to iCSI-based RBD. However, the latter approach requires accurate CSI knowledge of all channel links involved, which is costly in terms of the amount of training required, especially when dealing with large RISs.

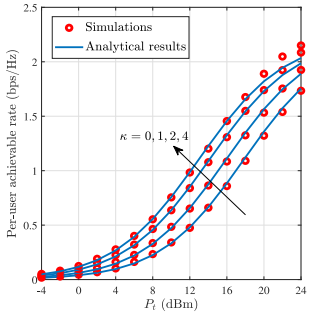

Fig. 2. Per-user achievable rate versus transmit power under different levels of VM noise concentration parameter (κ) when $|\rho| = 0.8$, $N_1 = N_2 = 100$, and $M = 64$.

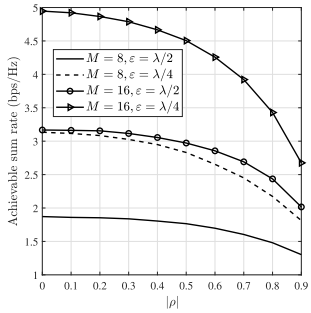

Fig. 3. Achievable sum rate versus $|\rho|$ for different number of BS antennas (M) when $N_1 = N_2 = 100$, $P_t = 20$ dBm, and $\kappa = 4$.

any real number, and $\mathbf{1}_{N_i}$ is a vector of length N_i with entries of all ones.

Proof: By examining the structure of $v_i = \text{tr}(\boldsymbol{R}_i \boldsymbol{\Theta}_i \boldsymbol{R}_i \boldsymbol{\Theta}_i^H)$, and keeping in mind that $\boldsymbol{R}_i$ is a Hermitian matrix, and the trace of a square matrix is the sum of its diagonal, we can express v_i as

$$v_i = \sum_{n=1}^{N_i} \sum_{l=1}^{N_i} \left| [\boldsymbol{R}_i]_{n,l} \right|^2 e^{\jmath([\boldsymbol{\theta}_i]_l - [\boldsymbol{\theta}_i]_n)}. \tag{10}$$

Clearly, v_i is maximum only when $[\boldsymbol{\theta}_i^\star]_l = [\boldsymbol{\theta}_i^\star]_n$, which means that all phase-shifts at each RIS should have equal values, i.e., $([\boldsymbol{\theta}_i^\star]_1 = [\boldsymbol{\theta}_i^\star]_2 = \cdots\cdots = [\boldsymbol{\theta}_i^\star]_{N_i})$.

Theorem 2 means that for correlated Rayleigh fading, there are infinite solutions of optimal phase-shifts, and each solution can be easily generated without any sophisticated optimization tools. It follows that under optimal RBD, the expression for η_k corresponding to the optimal achievable rate becomes

$$\begin{aligned} \eta_k^\star = \beta_{B1}\beta_{2k}\beta_G \Big[\text{tr}\Big(\boldsymbol{R}_2^2\Big) \Big(\varphi^4 \text{tr}\Big(\boldsymbol{R}_1^2\Big) + (\varphi^2 - \varphi^4) N_1\Big) \\ + N_2 \Big((\varphi^2 - \varphi^4) \text{tr}\Big(\boldsymbol{R}_1^2\Big) + (1 - \varphi^2)^2 N_1 \Big) \Big] \\ + \sum_{i=1}^{2} \beta_{Bi}\beta_{ik} \Big(\varphi^2 \text{tr}\Big(\boldsymbol{R}_i^2\Big) + (1 - \varphi^2) N_i \Big). \end{aligned} \tag{11}$$

Remark 3: Noting that the values in the off-diagonal of $\boldsymbol{R}_i$ reflect the amount of correlation between two reflecting elements at I_i, such that the higher the correlation the larger these values become, (11) clearly demonstrates that a higher spatial correlation at each RIS results in higher $\eta_k^\star$ (and thus higher achievable rate), since $\text{tr}(\boldsymbol{R}_i^2)$ is the sum of all elements in $\boldsymbol{R}_i$ squared, which proves our previous statement in Remark 1. Considering two extreme cases, if no correlation existed at $\boldsymbol{R}_i$ (i.e., $\boldsymbol{R}_i = \boldsymbol{I}_{N_i}$), then $\text{tr}(\boldsymbol{R}_i^2)$ would be equal to N_i. In contrast, if full correlation existed such that all the off-diagonal elements of $\boldsymbol{R}_i$ are equal to one,[7] then $\text{tr}(\boldsymbol{R}_i^2) = N_i^2$.

IV. Results and Discussion

We start by defining the simulation setup. The BS is located at the origin of a 2D plane such that $(x_{\text{BS}}, y_{\text{BS}}) = (0, 0)$, while $(x_{I_1}, y_{I_1}) = (0, 15)$, $(x_{I_2}, y_{I_2}) = (60, 15)$, all in meters, and the K users are located over a straight line between (50, 0) and (70, 0), such that $(x_{U_k}, y_{U_k}) = (50 + \frac{k-1}{K-1} \times 20, 0)$, $\forall k \in \mathcal{U}$. Unless stated otherwise, we also set $\lambda = 0.1$m, $d_V = d_H = \lambda/4$, $\alpha = 2.7$, RIS element spacing $\varepsilon = \lambda/4$, $\sigma^2 = -94$ dBm, and $K = 4$. Finally, equal power allocation has been adopted among all users, and optimal RBD was utilized such that $\boldsymbol{\Theta}_i = \text{diag}\{\mathbf{1}_{N_i}\}$.

Fig. 2 demonstrates the average per-user achievable rate performance. As one would expect, a larger transmit power budget at the BS leads to a higher achievable rate. In addition, the results also highlight the effect of phase-noise on the performance. In particular, higher values of κ means that the distribution of the VM phase-noise is more centered around its mean, thereby allowing better phase-adjustment capabilities at both RISs and thus higher achievable rates. It is also worth highlighting that the analytical results closely match the ones obtained via computer simulations, which validate our closed-form expressions and prove their accuracy.

Fig. 3 illustrates the effects of spatial correlation at both RISs as well as BS. The presented results firmly confirm our statements regarding the opposite roles of spatial correlation at BS and RISs for the considered MU-MISO network scenario, as indicated in both (7) and (11). More specifically, the results in Fig. 3 clearly show that higher spatial correlation at BS is not desired, while the opposite holds for the correlation at RISs (note that smaller element spacing ϵ means higher correlation at RIS). These observations indicate that for practical implementations, the miniaturization of RIS is highly desirable, as it leads to higher achievable rates due to the increased spatial correlation. Finally, as expected and also indicated by (7), increasing the number of BS antennas M can largely enhance the achievable rate performance.

V. Conclusion

We investigated the performance of a phase-noise impaired double-RIS MU-MISO network over spatially correlated channels. Closed-form expressions were derived for both the downlink achievable rate and optimal reflect beamforming design under MRT precoding scheme. Our results provided insight into the effects of phase-noise and spatial correlation at BS and RISs. In particular, it was observed that high spatial correlation is preferred at RISs, but not the BS, to achieve higher rates. Numerical results closely matched the analytical expressions which proved the validity and accuracy of our analysis.

Appendix

We start by introducing the lower-bound expression of the ergodic SINR, which relies on *channel hardening*. In particular, considering the kth user, we have [13]

$$\begin{aligned} \underline{\text{SINR}}_k &= \frac{p_k \left| \mathbb{E}\left\{ \boldsymbol{h}_k^T \boldsymbol{w}_k \right\} \right|^2}{\sum_{l \in \mathcal{U}} p_l \mathbb{E}\left\{ \left| \boldsymbol{h}_k^T \boldsymbol{w}_l \right|^2 \right\} - p_k \left| \mathbb{E}\left\{ \boldsymbol{h}_k^T \boldsymbol{w}_k \right\} \right|^2 + \text{Var}\{z_k\}} \\ &\overset{\text{a}_0}{=} \frac{p_k \text{tr}(\boldsymbol{\Psi}_k)}{\sum_{l \in \mathcal{U}} p_l \frac{\text{tr}(\boldsymbol{\Psi}_k \boldsymbol{\Psi}_l)}{\text{tr}(\boldsymbol{\Psi}_l)} + \sigma^2}, \end{aligned} \tag{12}$$

[7] Please note that such a case is only hypothetical and cannot exist in reality, as it indicates that all elements share the exact same physical location.

where $\boldsymbol{\Psi}_k$ is the channel covariance matrix for kth user, and the equality (a_0) holds only for the adopted MRT beamforming. Note that according to the central limit theorem, the cascaded channel admits to complex Gaussian distribution when N_1 and N_2 are large, and thus [13, Lemma B.14] can be applied to obtain the expression in (12).

Next, we derive the channel covariance matrix of kth user. In particular, we have

$$\begin{aligned}\boldsymbol{\Psi}_k &= \mathbb{E}\Big\{\boldsymbol{h}_k\boldsymbol{h}_k^H\Big\}\\ &= \mathbb{E}\Big\{\boldsymbol{H}_{B1}\tilde{\boldsymbol{\Theta}}_1\boldsymbol{G}\tilde{\boldsymbol{\Theta}}_2\boldsymbol{q}_{2k}\boldsymbol{q}_{2k}^H\tilde{\boldsymbol{\Theta}}_2^H\boldsymbol{G}^H\tilde{\boldsymbol{\Theta}}_1^H\boldsymbol{H}_{B1}^H\\ &\quad+\boldsymbol{H}_{B1}\tilde{\boldsymbol{\Theta}}_1\boldsymbol{q}_{1k}\boldsymbol{q}_{1k}^H\tilde{\boldsymbol{\Theta}}_1^H\boldsymbol{H}_{B1}^H+\boldsymbol{H}_{B2}\tilde{\boldsymbol{\Theta}}_2\boldsymbol{q}_{2k}\boldsymbol{q}_{2k}^H\tilde{\boldsymbol{\Theta}}_2^H\boldsymbol{H}_{B2}^H\\ &\quad+2\Re\Big\{\boldsymbol{H}_{B1}\tilde{\boldsymbol{\Theta}}_1\boldsymbol{q}_{1k}\boldsymbol{q}_{2k}^H\tilde{\boldsymbol{\Theta}}_2^H\boldsymbol{G}^H\tilde{\boldsymbol{\Theta}}_1^H\boldsymbol{H}_{B1}^H\Big\}\\ &\quad+2\Re\Big\{\boldsymbol{H}_{B2}\tilde{\boldsymbol{\Theta}}_2\boldsymbol{q}_{2k}\boldsymbol{q}_{2k}^H\tilde{\boldsymbol{\Theta}}_2^H\boldsymbol{G}^H\tilde{\boldsymbol{\Theta}}_1^H\boldsymbol{H}_{B1}^H\Big\}\\ &\quad+2\Re\Big\{\boldsymbol{H}_{B2}\tilde{\boldsymbol{\Theta}}_2\boldsymbol{q}_{2k}\boldsymbol{q}_{1k}^H\tilde{\boldsymbol{\Theta}}_1^H\boldsymbol{H}_{B1}^H\Big\}\Big\}. \end{aligned}\tag{13}$$

In the following, we evaluate the expectation of each term in (13) separately. Specifically, for the first term, we have

$$\begin{aligned}&\mathbb{E}\Big\{\boldsymbol{H}_{B1}\tilde{\boldsymbol{\Theta}}_1\boldsymbol{G}\tilde{\boldsymbol{\Theta}}_2\boldsymbol{q}_{2k}\boldsymbol{q}_{2k}^H\tilde{\boldsymbol{\Theta}}_2^H\boldsymbol{G}^H\tilde{\boldsymbol{\Theta}}_1^H\boldsymbol{H}_{B1}^H\Big\}\\ &=\beta_{2k}\mathbb{E}\Big\{\boldsymbol{H}_{B1}\tilde{\boldsymbol{\Theta}}_1\boldsymbol{G}\tilde{\boldsymbol{\Theta}}_2\boldsymbol{R}_2^{\frac{1}{2}}\tilde{\boldsymbol{q}}_{2k}\tilde{\boldsymbol{q}}_{2k}^H\boldsymbol{R}_2^{\frac{1}{2}}\tilde{\boldsymbol{\Theta}}_2^H\boldsymbol{G}^H\tilde{\boldsymbol{\Theta}}_1^H\boldsymbol{H}_{B1}^H\Big\}\\ &=\beta_{2k}\mathbb{E}\Big\{\boldsymbol{H}_{B1}\tilde{\boldsymbol{\Theta}}_1\boldsymbol{G}\bar{\boldsymbol{\Theta}}_2\boldsymbol{\Theta}_2\boldsymbol{R}_2\boldsymbol{\Theta}_2^H\bar{\boldsymbol{\Theta}}_2^H\boldsymbol{G}^H\tilde{\boldsymbol{\Theta}}_1^H\boldsymbol{H}_{B1}^H\Big\}\\ &\overset{\mathrm{a}_1}{=}\beta_{2k}\mathbb{E}\Big\{\boldsymbol{H}_{B1}\tilde{\boldsymbol{\Theta}}_1\boldsymbol{G}\Big(\varphi^2\bar{\boldsymbol{R}}_2+(1-\varphi^2)\boldsymbol{I}_{N_2}\Big)\boldsymbol{G}^H\tilde{\boldsymbol{\Theta}}_1^H\boldsymbol{H}_{B1}^H\Big\}\\ &=\beta_{2k}\Big(\varphi^2\boldsymbol{A}+(1-\varphi^2)\boldsymbol{B}\Big),\end{aligned}\tag{14}$$

where $\bar{\boldsymbol{R}}_2 = \boldsymbol{\Theta}_2\boldsymbol{R}_2\boldsymbol{\Theta}_2^H$, and equality (a_1) holds from [9, eq. (13)]. Furthermore, we have

$$\begin{aligned}\boldsymbol{A} &= \mathbb{E}\Big\{\boldsymbol{H}_{B1}\tilde{\boldsymbol{\Theta}}_1\boldsymbol{G}\bar{\boldsymbol{R}}_2\boldsymbol{G}^H\tilde{\boldsymbol{\Theta}}_1^H\boldsymbol{H}_{B1}^H\Big\}\\ &=\beta_G\mathbb{E}\Big\{\boldsymbol{H}_{B1}\tilde{\boldsymbol{\Theta}}_1\boldsymbol{R}_1^{\frac{1}{2}}\tilde{\boldsymbol{G}}\boldsymbol{R}_2^{\frac{1}{2}}\bar{\boldsymbol{R}}_2\boldsymbol{R}_2^{\frac{1}{2}}\tilde{\boldsymbol{G}}^H\boldsymbol{R}_1^{\frac{1}{2}}\tilde{\boldsymbol{\Theta}}_1^H\boldsymbol{H}_{B1}^H\Big\}\\ &=\beta_G\mathrm{tr}\big(\boldsymbol{R}_2\bar{\boldsymbol{R}}_2\big)\mathbb{E}\Big\{\boldsymbol{H}_{B1}\bar{\boldsymbol{\Theta}}_1\boldsymbol{\Theta}_1\boldsymbol{R}_1\boldsymbol{\Theta}_1^H\bar{\boldsymbol{\Theta}}_1^H\boldsymbol{H}_{B1}^H\Big\}\\ &=\beta_G\mathrm{tr}\big(\boldsymbol{R}_2\bar{\boldsymbol{R}}_2\big)\mathbb{E}\Big\{\boldsymbol{H}_{B1}\big(\varphi^2\bar{\boldsymbol{R}}_1+(1-\varphi^2)\boldsymbol{I}_{N_1}\big)\boldsymbol{H}_{B1}^H\Big\}\\ &=\beta_G\mathrm{tr}\big(\boldsymbol{R}_2\bar{\boldsymbol{R}}_2\big)\Big(\varphi^2\mathbb{E}\Big\{\boldsymbol{H}_{B1}\bar{\boldsymbol{R}}_1\boldsymbol{H}_{B1}^H\Big\}\\ &\quad+(1-\varphi^2)\mathbb{E}\Big\{\boldsymbol{H}_{B1}\boldsymbol{H}_{B1}^H\Big\}\Big)\\ &=\beta_G\mathrm{tr}\big(\boldsymbol{R}_2\bar{\boldsymbol{R}}_2\big)\Big(\varphi^2\beta_{B1}\mathbb{E}\Big\{\boldsymbol{R}_B^{\frac{1}{2}}\tilde{\boldsymbol{H}}_{B1}\boldsymbol{R}_1^{\frac{1}{2}}\bar{\boldsymbol{R}}_1\boldsymbol{R}_1^{\frac{1}{2}}\tilde{\boldsymbol{H}}_{B1}^H\boldsymbol{R}_B^{\frac{1}{2}}\Big\}\\ &\quad+(1-\varphi^2)\beta_{B1}\mathbb{E}\Big\{\boldsymbol{R}_B^{\frac{1}{2}}\tilde{\boldsymbol{H}}_{B1}\boldsymbol{R}_1\tilde{\boldsymbol{H}}_{B1}^H\boldsymbol{R}_B^{\frac{1}{2}}\Big\}\Big)\\ &=\beta_{B1}\beta_G\mathrm{tr}\big(\boldsymbol{R}_2\bar{\boldsymbol{R}}_2\big)\big(\varphi^2\mathrm{tr}\big(\boldsymbol{R}_1\bar{\boldsymbol{R}}_1\big)+(1-\varphi^2)\mathrm{tr}\big(\boldsymbol{R}_1\big)\big)\boldsymbol{R}_B,\end{aligned}\tag{15}$$

where $\bar{\boldsymbol{R}}_1 = \boldsymbol{\Theta}_1\boldsymbol{R}_1\boldsymbol{\Theta}_1^H$, and the properties $\mathrm{tr}(\boldsymbol{X}\,Y) = \mathrm{tr}(\boldsymbol{Y}\,X)$, and $\mathbb{E}\{\boldsymbol{V}\,\boldsymbol{U}\,\boldsymbol{V}^H\} = \mathrm{tr}(\boldsymbol{U})\boldsymbol{I}_{d_1}$ were applied. The latter property holds for any matrix $\boldsymbol{V} \in \mathbb{C}^{d_1\times d_2}$ with i.i.d entries of zero mean and unit variance, and $\boldsymbol{U}$ being a deterministic square matrix with per-dimension size of d_2. Following similar steps, the value of $\boldsymbol{B}$ can be given as

$$\begin{aligned}\boldsymbol{B} &= \mathbb{E}\Big\{\boldsymbol{H}_{B1}\tilde{\boldsymbol{\Theta}}_1\boldsymbol{G}\boldsymbol{G}^H\tilde{\boldsymbol{\Theta}}_1^H\boldsymbol{H}_{B1}^H\Big\}\\ &=\beta_{B1}\beta_G\mathrm{tr}(\boldsymbol{R}_2)\Big(\varphi^2\mathrm{tr}\big(\boldsymbol{R}_1\bar{\boldsymbol{R}}_1\big)+(1-\varphi^2)\mathrm{tr}(\boldsymbol{R}_1)\Big)\boldsymbol{R}_B.\end{aligned}\tag{16}$$

Furthermore, for the second term in (13), we have

$$\begin{aligned}&\mathbb{E}\Big\{\boldsymbol{H}_{B1}\tilde{\boldsymbol{\Theta}}_1\boldsymbol{q}_{1k}\boldsymbol{q}_{1k}^H\tilde{\boldsymbol{\Theta}}_1^H\boldsymbol{H}_{B1}^H\Big\}\\ &=\beta_{B1}\beta_{1k}\Big(\varphi^2\mathrm{tr}\big(\boldsymbol{R}_1\bar{\boldsymbol{R}}_1\big)+(1-\varphi^2)\mathrm{tr}\big(\boldsymbol{R}_1\big)\Big)\boldsymbol{R}_B.\end{aligned}\tag{17}$$

Similarly, the third term is given as

$$\begin{aligned}&\mathbb{E}\Big\{\boldsymbol{H}_{B2}\tilde{\boldsymbol{\Theta}}_2\boldsymbol{q}_{2k}\boldsymbol{q}_{2k}^H\tilde{\boldsymbol{\Theta}}_2^H\boldsymbol{H}_{B2}^H\Big\}\\ &=\beta_{B2}\beta_{2k}\Big(\varphi^2\mathrm{tr}\big(\boldsymbol{R}_2\bar{\boldsymbol{R}}_2\big)+(1-\varphi^2)\mathrm{tr}\big(\boldsymbol{R}_2\big)\Big)\boldsymbol{R}_B.\end{aligned}\tag{18}$$

In contrast, the expected value for each of the last three terms in (13) is equal to zero due to the independence between $\boldsymbol{q}_{1k}$ and $\boldsymbol{q}_{2k}$, as well as between $\boldsymbol{H}_{B1}$ and $\boldsymbol{H}_{B2}$.

Next, we recall that $\mathrm{tr}(\boldsymbol{R}_i) = N_i$, and after re-arranging the expressions and substituting the results of (15) and (16) into (14), followed by adding the results of (14), (17) and (18), we obtain

$$\begin{aligned}\boldsymbol{\Psi}_k &= \Big[\beta_{B1}\beta_{2k}\beta_G\Big(\mathrm{tr}\big(\boldsymbol{R}_2\bar{\boldsymbol{R}}_2\big)\Big(\varphi^4\mathrm{tr}\big(\boldsymbol{R}_1\bar{\boldsymbol{R}}_1\big)+(\varphi^2-\varphi^4)N_1\Big)\\ &\quad+N_2\Big((\varphi^2-\varphi^4)\mathrm{tr}\big(\boldsymbol{R}_1\bar{\boldsymbol{R}}_1\big)+(1-\varphi^2)^2N_1\Big)\Big)\\ &\quad+\beta_{B1}\beta_{1k}\Big(\varphi^2\mathrm{tr}\big(\boldsymbol{R}_1\bar{\boldsymbol{R}}_1\big)+(1-\varphi^2)N_1\Big)\\ &\quad+\beta_{B2}\beta_{2k}\Big(\varphi^2\mathrm{tr}\big(\boldsymbol{R}_2\bar{\boldsymbol{R}}_2\big)+(1-\varphi^2)N_2\Big)\Big]\boldsymbol{R}_B\\ &=\eta_k\boldsymbol{R}_B.\end{aligned}\tag{19}$$

Finally, substituting the expression of $\boldsymbol{\Psi}_j$ $(j \in \{k,l\})$ into (12), and noting that $\mathrm{tr}(\boldsymbol{R}_B) = M$, the expression in (7) is obtained after straightforward mathematical manipulations.

REFERENCES

[1] C. Pan *et al.*, "Reconfigurable intelligent surfaces for 6G systems: Principles, applications, and research directions," *IEEE Commun. Mag.*, vol. 59, no. 6, pp. 14–20, Jun. 2021.

[2] Q. Wu and R. Zhang, "Towards smart and reconfigurable environment: Intelligent reflecting surface aided wireless network," *IEEE Commun. Mag.*, vol. 58, no. 1, pp. 106–112, Jan. 2020.

[3] C. Huang *et al.*, "Multi-hop RIS-empowered terahertz communications: A DRL-based hybrid beamforming design," *IEEE J. Sel. Areas Commun.*, vol. 39, no. 6, pp. 1663–1677, Jun. 2021.

[4] B. Zheng *et al.*, "Double-IRS assisted multi-user MIMO: Cooperative passive beamforming design," *IEEE Trans. Wireless Commun.*, vol. 20, no. 7, pp. 4513–4526, Jul. 2021.

[5] C. You *et al.*, "Wireless communication via double IRS: Channel estimation and passive beamforming designs," *IEEE Wireless Commun. Lett.*, vol. 10, no. 2, pp. 431–435, Feb. 2021.

[6] A. Papazafeiropoulos *et al.*, "Coverage probability of double-IRS assisted communication systems," *IEEE Wireless Commun. Lett.*, vol. 11, no. 1, pp. 96–100, Jan. 2022.

[7] M.-A. Badiu and J. P. Coon, "Communication through a large reflecting surface with phase errors," *IEEE Wireless Commun. Lett.*, vol. 9, no. 2, pp. 184–188, Feb. 2020.

[8] T. Wang *et al.*, "Outage probability analysis of RIS-assisted wireless networks with von Mises phase errors," *IEEE Wireless Commun. Lett.*, vol. 10, no. 12, pp. 2737–2741, Dec. 2021.

[9] A. Papazafeiropoulos *et al.*, "Intelligent reflecting surface-assisted MU-MISO systems with imperfect hardware: Channel estimation, beamforming design," *IEEE Trans. Wireless Commun.*, vol. 21, no. 3, pp. 2077–2092, Mar. 2022.

[10] A. Papazafeiropoulos *et al.*, "Asymptotic analysis of max–min weighted SINR for IRS-assisted MISO systems with hardware impairments," *IEEE Wireless Commun. Lett.*, early access, Jul. 8, 2021, doi: 10.1109/LWC.2021.3095678.

[11] Z. Xing *et al.*, "Achievable rate analysis and phase shift optimization on intelligent reflecting surface with hardware impairments," *IEEE Trans. Wireless Commun.*, vol. 20, no. 9, pp. 5514–5530, Sep. 2021.

[12] S. Zhou *et al.*, "Spectral and energy efficiency of IRS-assisted MISO communication with hardware impairments," *IEEE Wireless Commun. Lett.*, vol. 9, no. 9, pp. 1366–1369, Sep. 2020.

[13] E. Björnson *et al.*, "Massive MIMO networks: Spectral, energy, and hardware efficiency," *Found. Trends Signal Process.*, vol. 11, nos. 3–4, pp. 154–655, 2017.

[14] E. Björnson and L. Sanguinetti, "Rayleigh fading modeling and channel hardening for reconfigurable intelligent surfaces," *IEEE Wireless Commun. Lett.*, vol. 10, no. 4, pp. 830–834, Apr. 2020.

[15] K. Yu *et al.*, "Second order statistics of NLOS indoor MIMO channels based on 5.2 GHz measurements," in *Proc. IEEE GLOBECOM*, Nov. 2001, pp. 156–160.